Sensitivity of top-down CO source estimates to the modeled vertical structure in atmospheric CO

Zhe Jiang[1,2], Dylan B. A. Jones[1,3], Helen M. Worden[4], Daven K. Henze[5]

[1]Department of Physics, University of Toronto, Toronto, ON, Canada
[2] Now at Jet Propulsion Laboratory, California Institute of Technology, Pasadena CA, USA
[3]JIFRESSE, University of California, Los Angeles, Los Angeles, CA, USA
[4]National Center for Atmospheric Research, Boulder, CO, USA
[5]Department of Mechanical Engineering, University of Colorado Boulder, Boulder, CO, USA

Abstract

We assessed the sensitivity of regional CO source estimates to the modeled vertical CO distribution by assimilating multi-spectral MOPITT V5J CO retrievals with the GEOS-Chem model. We compared the source estimates obtained by assimilating the CO profiles and the surface layer retrievals from June 2004 to May 2005. Because the surface layer retrievals are less sensitive to CO in the free troposphere, it is expected that they should provide constraints in the CO source estimates that are less sensitive to the vertical structure of CO in the free troposphere. The inferred source estimates all suggest a reduction in CO emissions in the tropics and subtropics and an increase in the extratropics over the a priori estimates. The tropical decreases were particularly pronounced for regions where the biogenic source of CO was dominant, suggesting an overestimate of the a priori isoprene source of CO in the model. We found that the differences between the regional source estimates inferred from the profile and surface layer retrievals for 2004-2005 were small, generally less than 10% for the main continental regions, except for estimates for South Asia, North America, and Europe. Because of discrepancies in convective transport in the model, the CO source estimates for India and Southeast Asia inferred from the CO profiles were significantly higher than those estimated from the surface layer retrievals during June-August 2004. On the other hand, the profile inversion underestimated the CO emissions from North America and Europe compared to the assimilation of the surface layer retrievals. We showed that vertical transport of air from the North American and European boundary layer is slower than from other continental regions and thus air in the free troposphere from North America and Europe in the model is more chemically aged, which could explain the discrepancy between the source estimates inferred from the profile and surface layer retrievals. We also examined the impact of the OH distribution on the source estimates and found that the

discrepancies between the source estimates obtained with two OH fields were larger when using the profile data, which is consistent with greater sensitivity to the more chemically aged air in the free troposphere. Our findings indicate that regional CO source estimates are sensitive to the vertical CO structure. They suggest that diagnostics to assess the age of air from the continental source regions should help interpret the results from CO source inversions. Our results also suggest that assimilating a broader range of composition measurements to provide better constraint on tropospheric OH and the biogenic sources of CO is essential for reliable quantification of the regional CO budget.

1. Introduction

The emissions of greenhouse gases and other atmospheric pollutants have been significantly increased since the industrial revolution. Their influences on atmospheric chemical composition, local air quality and climate are the subject of increasing numbers of studies. In this context, inverse modeling has been widely used to provide better understanding of the emissions of these atmospheric constituents. In particular, in the past decade there has been expanded use of inverse modeling to better quantify the emissions of atmospheric CO (e.g., Pétron et al., 2004; Heald et al., 2004; Arellano et al., 2006; Jones et al., 2009; Kopacz et al., 2010; Fortems-Cheiney et al., 2011; Gonzi et al., 2011). Tropospheric CO is produced from incomplete combustion and is a byproduct of oxidation of hydrocarbons. As the primary sink of OH, tropospheric CO has significant influence on the oxidative capacity of the atmosphere. The lifetime of tropospheric CO is a few months, which is long enough to track within intercontinental scale pollution plumes but short enough to provide strong signals over background distribution (Jiang et al., 2010). Previous studies (Palmer et al., 2006; Wang et al., 2009) have demonstrated that CO can be included in the inverse analyses of CO_2 sources and sinks to reduce the influence of model

transport errors.

Remote sensing from space-based instruments provide valuable global observational coverage to enable us to better constrain CO emissions. There are now several satellite sensors from which abundances of CO in the troposphere have been retrieved using measurement of thermal infrared (TIR) radiation near 4.7 μm: MOPITT (Measurements of Pollution In The Troposphere), on EOS-Terra, launched December 1999 (Deeter et al., 2003); AIRS (Atmospheric InfraRed Sounder), on EOS-Aqua, launched May, 2002 (Warner et al., 2007); TES, (Tropospheric Emission Spectrometer) on EOS-Aura, launched July, 2004 (Luo et al., 2007); and IASI (Infrared Atmospheric Sounding Interferometer), on METOP-A, launched October, 2006 (George et al., 2009). The TIR radiances are sensitive to CO concentrations from the middle to the upper troposphere. The lack of global observations of CO near the surface has implications for the use of inverse modeling to quantify CO emissions because the modeled CO distribution in the free troposphere is affected by discrepancies in the parameterization of convective transport in models (e.g. Ott et al., 2009), the simulated chemical sink of CO (e.g. Jiang et al. 2011), and long-range transport (e.g. Arellano et al. 2006b; Jiang et al., 2013).

The multispectral MOPITT version 5 CO product (V5J, where J indicates joint retrievals) are the first retrievals to exploit simultaneous near infrared (NIR) and TIR measurement to provide greater sensitivity to CO in the lower troposphere over land (Deeter et al., 2011). Recently, Jiang et al. (2013) showed that lower tropospheric MOPITT V5J CO retrievals can be used to study the influence of convective transport error on CO source estimates. They compared the CO source estimates in June-August 2006, inferred from MOPITT surface layer retrievals, the profile retrievals, and the column amounts. They found that there were large discrepancies in the inferred source estimates obtained with the surface layer and profile retrievals in Asian

93 monsoon regions where strong emissions are co-located with significant vertical mass flux due to
94 convection. The discrepancies in the CO source estimates were also used to assess the impact of
95 vertical transport error on the CH_4 emission estimates from Indonesian peat fires in fall 2006,
96 estimated from TES CH_4 observations (Worden et al., 2013).

97 The study by Jiang et al. (2013) was carried only for summer 2006 and focused mainly
98 on discrepancies in convective transport. The work presented here complements and extends that
99 analysis. Reflecting its long lifetime, CO is destroyed mainly in the free troposphere rather than
100 in the boundary layer. Thus, free tropospheric CO will be more susceptible to discrepancies in
101 OH, and in long-range transport. One way to mitigate the potential impact of discrepancies in
102 transport and OH on CO inversion analyses is to use surface observations, near the CO source
103 regions. However, the current surface-observing network is sparse, whereas MOPITT provides
104 significantly greater observational coverage. Therefore, we focus here on the use of the surface
105 layer retrievals from MOPITT for inverse modeling CO sources. We expect that the source
106 estimates inferred from the surface layer retrievals will be less sensitive to errors in OH and
107 model transport. We estimate and compare monthly CO source estimates for June 2004 to May
108 2005 using MOPITT tropospheric profiles and surface layer retrievals to observe the influence of
109 the OH distribution and the vertical structure in CO, as observed by MOPITT, on the inferred
110 source estimates. The updated global CO distributions will be used as boundary conditions in our
111 companion paper to constrain the North America CO emission at a horizontal resolution of
112 0.5°x0.67° (Jiang et al., 2014). The objective of that study is to assess the extent to which we can
113 further reduce the impact of model transport and chemistry errors on CO source estimates in a
114 regional inverse modeling context.

115 This paper is organized as follows: in Section 2 we describe the MOPITT instruments

and the GEOS-Chem model used in this work. In Section 3 we outline the inverse method. We then discuss the annual and seasonal variations of the estimated CO emissions in Section 4. The discrepancies in the CO source estimates are interpreted in the context of the CO vertical structure and the OH distribution. Our conclusions follow in Section 5. In Appendix A we present the results of an indirect validation of the MOPITT data that was conducted to guide the filtering of the data used in the assimilation, and in Appendix B we have included a discussion of the optimization scheme used in the assimilation.

2. Observations and Model

2.1. MOPITT

The MOPITT instrument was launched on the Terra spacecraft on December 18, 1999. The satellite is in a sun-synchronous polar orbit of 705 km and crosses the equator at 10:30 local time. With a footprint of 22 km *x* 22 km, the instrument makes measurements in a 612 km cross-track scan that provides global coverage every three days. The MOPITT data used here were obtained from the joint retrieval of CO from TIR (4.7μm) and NIR (2.3μm) radiances using an optimal estimation approach (Worden et al., 2010; Deeter et al., 2011). The retrieved volume mixing ratios (VMR) are reported as layer averages 10 pressure levels (surface, 900, 800, 700, 600, 500, 400, 300, 200 and 100 hPa) and the relationship between the retrieved CO profile and the true atmospheric state can be expressed as:

$$\hat{\mathbf{z}} = \mathbf{z}_a + \mathbf{A}(\mathbf{z} - \mathbf{z}_a) + \mathbf{G}\varepsilon \quad (1)$$

where $\mathbf{z}_a$ is the MOPITT a priori CO profile (expressed as log(VMR)), $\mathbf{z}$ is the true atmospheric state averaged at MOPITT grid levels (also as log(VMR)), $\mathbf{G}\varepsilon$ describes the retrieval error, and $\mathbf{A} = \partial\hat{\mathbf{z}}/\partial\mathbf{z}$ is the MOPITT averaging kernel matrix, which gives the sensitivity of the retrieval to

the actual CO in the atmosphere. The MOPITT V5 data have been evaluated by Deeter et al. (2012, 2013) using aircraft measurements from the National Oceanic and Atmospheric Administration (NOAA). For the V5J multi-spectral retrievals, they found a small positive bias of 2.7% at the surface and a much larger positive bias of 14% at 200 hPa. As a result of the high bias in the upper troposphere, in our analysis we do not use the retrievals at altitudes above 200 hPa. We conduced an indirect validation of the MOPITT V5J data (see Appendix A) using NOAA Global Monitoring Division (GMD) in situ observations, which suggested that there is a high-latitude positive bias in the MOPITT data, possibly associated with the lower degrees-of-freedom-for-signal (DFS) at higher latitudes. Consequently, in this work, we omitted MOPITT data that are polarward of 40° over oceans and 52° over land.

2.2. GEOS-Chem

The GEOS-Chem global chemical transport model (CTM) [www.geos-chem.org] is driven by assimilated meteorological fields from the NASA Goddard Earth Observing System (GEOS-5) at the Global Modeling and data Assimilation Office. We use version v34 of the GEOS-Chem adjoint, which is based on v8-02-01 of the forward GEOS-Chem model, with relevant updates through v9-01-01. Our analysis is conducted at a horizontal resolution of 4°x5° and employs the CO-only simulation in GEOS-Chem, which uses archived monthly OH fields from the full chemistry simulation. The standard OH fields used in this work are from GEOS-Chem version v5-07-08, with a global annual mean OH concentration of 0.99×10^6 molec/cm^3 (Evans et al. 2005). We use this as our standard OH field to facilitate comparison of our results with those of Kopacz et al. (2010). We also conduct a sensitivity analysis using OH fields from the full chemistry simulation of v34 of the adjoint model, run in forward mode. This simulation produces a global annual mean OH concentration of 1.24×10^6 molec/cm^3.

161 The anthropogenic emission inventories are identical to those used in Jiang et al. (2013).
162 Anthropogenic emissions are from EDGAR 3.2FT2000 (Olivier et al., 2001), but are replaced by
163 the following regional emission inventories: the US Environmental Protection Agency National
164 Emission Inventory (NEI) for 2005 in North America, the Criteria Air Contaminants (CAC)
165 inventory for Canada, the Big Bend Regional Aerosol and Visibility Observational (BRAVO)
166 Study Emissions Inventory for Mexico (Kuhns et al., 2003), the Cooperative Program for
167 Monitoring and Evaluation of the Long-range Transmission of Air Pollutants in Europe (EMEP)
168 inventory for Europe in 2000 (Vestreng et al., 2002) and the INTEX-B Asia emissions inventory
169 for 2006 (Zhang et al., 2009). Biomass burning emissions are based on the Global Fire Emission
170 Database (GFED3), with a three-hour temporal resolution (van der Werf et al., 2010). Additional
171 CO sources come from oxidation of methane and biogenic volatile organic compounds (VOCs,)
172 as described in previous studies (Kopacz et al., 2010; Jiang et al., 2013). The biogenic emissions
173 are simulated using the Model of Emissions of Gases and Aerosols from Nature, version 2.0
174 (MEGANv2.0) (Guenther et al., 2006). The distribution of the annual mean CO emissions for
175 June 2004 to May 2005 is shown in Figure 1. The annual global sources are 928 Tg CO from
176 fossil fuel, biofuel and biomass burning, 661 Tg CO from the oxidation of biogenic NMVOCs,
177 and 884 Tg CO from the oxidation of CH_4.

178 ## 3. Inversion Approach

179 We use the 4-dimensional variational (4D-var) data assimilation system in GEOS-Chem
180 (e.g., Henze et al., 2007; Kopacz et al., 2009, 2010; Singh et al. 2011; Jiang et al., 2011, 2013;
181 Parrington et al., 2012) to estimate the CO sources. Details of the 4D-var scheme are given in
182 Henze et al. (2007) and Kopacz et al. (2009, 2010). In this approach, we minimize the cost
183 function of the form,

$$J(\mathbf{x}) = \sum_{i=1}^{N} (\mathbf{F}_i(\mathbf{x}) - \mathbf{z}_i)^{\mathrm{T}} \mathbf{S}_{\Sigma}^{-1} (\mathbf{F}_i(\mathbf{x}) - \mathbf{z}_i) + (\mathbf{x} - \mathbf{x}_{\mathbf{a}})^{\mathrm{T}} \mathbf{S}_{\mathbf{a}}^{-1} (\mathbf{x} - \mathbf{x}_{\mathbf{a}}) \quad (2)$$

where $\mathbf{x}$ is the state vector of CO emissions, N is the number of MOPITT observations that are distributed in time over the assimilation period, $\mathbf{z}_i$ is a given MOPITT profile (or surface level retrieval), and $\mathbf{F(x)}$ is the forward model which represents the transport and chemistry of CO in the GEOS-Chem model and accounts for the vertical smoothing of the MOPITT retrieval,

$$\mathbf{F}_i(\mathbf{x}) = \mathbf{z}_a + \mathbf{A}(\mathbf{H}_i(\mathbf{x}) - \mathbf{z}_a) \quad (3)$$

Here $\mathbf{z}_a$ and $\mathbf{A}$ are the MOPITT a priori profile and averaging kernel, respectively, introduced in Equation (1), and $\mathbf{H}_i(\mathbf{x})$ is the GEOS-Chem profile of CO at the MOPITT observation location and time. The definition of the cost function assumes that the distribution of the errors for both the state vector $\mathbf{x}$ and the a priori constraint on the CO emissions $\mathbf{x}_a$ are Gaussian, and these errors are given by $\mathbf{S}_{\Sigma}$, the observational error covariance matrix, and $\mathbf{S}_{\mathbf{a}}$, the a priori error covariance matrix, respectively. Minimization of the cost function provides the a posteriori CO emissions $\hat{\mathbf{x}}$, corresponding to the maximum of the conditional probability density function ($P(\mathbf{x}|\mathbf{y})$), with the a posteriori error covariance matrix $\hat{\mathbf{S}}$. However, because the 4D-var optimization scheme does not store the full Hessian matrix, it is difficult to construct the a posteriori error covariance matrix, which is the inverse of the Hessian. Details of the optimization approach are given in Appendix B.

We employ a similar procedure for data processing and quality control as in our previous study, Jiang et al. (2013). Since MOPITT V5J CO retrievals have a positive bias at high altitudes (Deeter et al. 2013), our analysis is restricted to CO retrievals below 200 hPa. Following Jiang et al. (2013), we also reject MOPITT data with CO column amounts less than 5×10^{17} molec/cm^2

205 and use only daytime data. The threshold of $5x10^{17}$ molec/cm^2 was selected to prevent
206 unrealistically low CO columns from adversely impacting the inversion analyses.

207 The observation error $\mathbf{S}_\Sigma$ represents a sum of the retrieval errors, representativeness errors,
208 and random model errors. Using the Relative Residual Error (RRE) approach (Palmer et al.,
209 2003; Heald et al., 2004), which assumes that the mean differences between the model and
210 observations are due to discrepancies in the emissions while the residual reflects the observation
211 error, Kopacz et al. (2010) estimated that the observation errors for the MOPITT columns are 10%
212 - 30%. Although the RRE approach does not account for systematic model errors, it provides a
213 possible estimate of the random component of the observation errors. Accurately characterizing
214 the systematic errors (in the model and observations) is a challenge. Keller et al. (Quantifying
215 Model Biases in CO Emission Estimation Using Weak Constraint 4D-var, manuscript in
216 preparation) have assimilated MOPITT V5J data using a weak-constraint 4D-var scheme to
217 characterize the systematic component of the observation error. Their results suggest that the
218 weak-constraint 4D-var is a promising approach for accounting for systematic errors, but it is
219 still challenging. In the absence of meaningful information about the systematic errors in the
220 model for the period considered here, we do not account for systematic errors in minimizing the
221 cost function. Following Jiang et al. (2011, 2013), we assume a uniform observation error of
222 20%. Our assumed 20% error likely overestimates the observation error in the upper troposphere
223 and underestimates it near the surface.

224 As described in Jiang et al. (2013), we combine the combustion CO sources (fossil fuel,
225 biofuel and biomass burning) with the CO from the oxidation of biogenic NMVOCs and solve
226 for the total CO emissions in each grid box, assuming a 50% uniform a priori error and that the
227 errors are uncorrelated. We optimize the source of CO from the oxidation of methane separately

as an aggregated global source, assuming an a priori uncertainty of 25%. As in Jiang et al. (2013), we produce initial conditions at the beginning of each monthly assimilation window by assimilating MOPITT V5J data using a sequential sub-optimal Kalman filter (Parrington et al. 2008). For the results presented here, the Kalman filter assimilation was carried out from January 1, 2004, to May 1, 2005, and to optimize the CO distribution, which was archived at the beginning of each month. In the monthly inversion using the 4D-var system, the optimized CO distribution from the Kalman filter was read at the beginning of each month to obtain initial conditions. Consequently, the initial conditions for the model simulation are independent of the inverse analyses. Although we use a one-month assimilation window, it is possible that a longer window of two or three months would lead to greater constraints on the CO source estimates. However, as we will show below, the inversion is sensitive to the specified OH distribution and thus with a longer assimilation window would be more susceptible to discrepancies in the CO chemical sink.

4. Results and Discussion

4.1. CO Source Estimates for June 2004 – May 2005

Figures 2a and 2f show the annual mean emission scaling factors for June 2004 to May 2005, obtained using the MOPITT surface layer and profile retrievals, respectively. Both analyses suggest that CO emissions in the tropics should be reduced, whereas the emissions in middle and high latitudes should be increased. However, as shown in Figure 2k, the a posteriori scaling factors from profile inversion is higher in India and Southeast Asia. As discussed in Jiang et al. (2013), these descrepancies over India and Southeast Asia are likely due to model errors in convection transport. The profile inversion also produces larger emissions in parts of tropical Africa and northern South America. In general, however, the a posteriori emissions from the

profile inversion are lower than those obtained from the surface layer inversion, particularly at middle and high latitudes.

Table 1 shows the annual mean regional CO emissions from June 2004 to May 2005, inferred from the surface layer and profile retrievals. In this work, only the total CO emission is optimized in each grid box, but because the different CO source types have different spatial and temporal distributions, we apply the scaling factors in each grid box to each source type, which can provide useful information on the individual source types. As shown in Table 1, the emission reductions in the tropics and subtropics reflect large reductions in the biogenic source of CO, suggesting that our a priori biogenic emissions are too high. For example, in South America, with the profile inversion the biogenic source was reduced by 32%, whereas the combustion source was reduced by 13%. In northern Africa the biogenic source was reduced by 26% and the combustion source was reduced by 20% with the profile inversion. In the 48 contiguous United States the biogenic source was reduced by 31%, whereas the combustion source was increased by 5%. The reductions in the biogenic emissions were smaller in the surface layer inversion, but were still large for South America and northern Africa, 27% and 28%, respectively. We note that although there are large differences between the regional source estimates inferred from the profile and surface layer retrievals, the global total a posteriori CO emissions estimated from the two sets of retrievals are similar, 1513 Tg CO and 1555 Tg CO, respectively.

The seasonal mean scaling factors are shown in Figure 2. The main seasonal feature in the figure is that the inversions tend to decrease CO emission in the summer hemisphere and increase them in the winter hemisphere, with the profile inversion producing larger reductions (2b and 2g) and smaller increases (Figures 2d and 2i). Consequently, the differences between the scaling factors from the surface and profile inversions are smaller in winter. This pattern is

consistent with an overestimate of isoprene emissions and a possible underestimate of wintertime fossil fuel combustion (Stein et al. 2014). The overestimate of biogenic emissions in GEOS-Chem by MEGANv2.0 has been reproted by previous studies (Barkley et al., 2008; Millet et al., 2008; Liu et al., 2010). Millet et al., (2008) found that North American isoprene emissions estimated by MEGAN were greater than those inferred from observations of formaldehyde (HCHO) from the Ozone Monitoring Instrument (OMI) by as much as 23%. Liu et al. (2010) used a newer version of MEGAN, version 2.1, which simulates lower isoprene emissions than version 2.0 (which is emloyed in our analysis), and found that it also produced an overestimate of CO from isoprene oxidation, particulalry in eastern South America. Marais et al. (2014) found that MEGANv2.1 ovestimated African isoprene emissions for 2005 – 2009 by 26% relative to those inferred from OMI data, primarily over the equatorial forests and the northern savannas.

Figure 3 shows the timeseries of the monthly mean source estimates for the 48 contiguous United States, Europe, East Asia, and India/Southeast Asia. For India/Southeast Asia, the dominant source of CO is biomass burning from Indonesia, which peaks in August - October, and from southeast Asia, which peaks in February - April. For the other regions, combustion of fossil fuels and biofuels provides the main annual source of CO. As we noted above, the tendency is for the inverse model to reduce the emissions in summer and increase them in winter, particularly in the United States and East Asia. In the profile inversion, the North American combustion emissions were reduced by about a factor of two in July and August 2004, whereas they were increased by 48% in January – March 2005. The summertime reduction of the North American combustion emissions was smaller than that obtained with the surface layer retrievals, whereas the wintertime increase was similar in both inversions. In Asia, both inversions produced comparable summertime reductions and wintertime increases in the combustion

297 emissions, with the emission estimates from the profile inversion being slightly lower in summer
298 and higher in winter. The seasonality of the European source estimates obatined from the surface
299 layer retrievals was much less pronounced than that obtained for North America and Asia, and
300 was consistently higher than those obatined from the profile inversion.

301 The seasonal variation of the a posteriori combustion emissions shown in Figure 3 is
302 consistent with the results of Kopacz et al. (2010). Using data from MOPITT, SCIAMACHY
303 (SCanning Imaging Absorption spectroMeter for Atmospheric CHartographY), and AIRS,
304 Kopacz et al. (2010) showed that the CO emissions from North America, Europe and East Asia
305 should be significantly increased in winter. There is also good agreement between the two
306 studies in the aggregated emissions in the extratropical northern hemisphere. The total combined
307 a posteriori combustion source from the United States, Alaska, Canada, Europe, and East Asia
308 was 515 Tg and 548 Tg from the profile and surface inversions, respectively. The corresponding
309 a posteriori estimate from Kopacz et al. (2010), was 520 Tg.

310 However, there are large differences in the region source estimates between our analysis
311 and that of Kopacz et al. (2010). For example, our annual combustion emission estimate for the
312 contiguous United States was 100 Tg from the profile inversion, whereas Kopacz et al. (2010)
313 inferred 50 Tg. We note that our total a posteriori combustion source estimates for North
314 America of 173 Tg CO and 156 Tg CO for the surface layer and profile inversions, respectively,
315 is comparable to the a posteriori estimate of 206 Tg CO obtained by Fortems-Cheiney et al.
316 (2012) from their inversion analysis of the MOPITT data for 2005. A significant difference
317 between our inverson and that of Kopacz et al. (2010) is that their a priori combustion source for
318 the United States was 40 Tg, whereas ours was 112 Tg. Their low a priori estimate was based on
319 the results of Hudman et al. (2008), who suggested a 60% reduction in anthropogenic emissions

in the United States as a result of an analysis of aircraft data in July – August 2004. The discrepancies in the regional source estimates between the results here and those of Kopacz et al. (2010) could also be related to differences in the configuration of the inversion analyses, such as the treatment of the initial conditions or vertical transport in the models. Our inversion analyses employed the GEOS-5 meteorological fields, whereas Kopacz et al. (2010) used GEOS-4. A significant factor could be the treatment of the biogenic source of CO. Here the biogenic sources are combined with the combustion sources and optimized at the resolution of the model. In contrast, Kopacz et al. (2010) aggregated the biogenic source with the methane source and optimized the global mean source from methane and VOC oxidation. As shown in Jiang et al. (2011), optimizing the VOC source at a lower resolution than the combustion emissions could result in an overadjustment of the combustion sources.

In general, we find that the regional source estimates inferred from the surface layer and profile retrievals are consistent, with relative differences of less than 10%, except for source estimates for North America (the United States, Alaska and Canada), Europe, and India/southeast Asia (see Table 1). The discrepancy between the source estimates for India/southeast Asia from the two inversions is linked to vertical transport by the Asian monsoon and was discussed by Jiang et al. (2013). In the next section, we present a passive tracer analysis to provide insight into the discrepancies between the source estimates from North America and Euope.

4.2. Ideal Tracer Experiments

It is surprising that Europe and North America (the United States and Canada) are the two regions, after India/southeast Asia, with the largest discrepancies between the source estimates inferred from the profile and surface layer inversions. To better understand how the

343 vertical transport of CO from these region could impact the inversions, we conducted an analysis
344 using an idealized CO-like tracer. We performed a tagged-CO simulation for the period June
345 2004 – May 2005 in which we imposed a constant source of CO of 3.33 Tg CO/day from each of
346 the continental source regions shown in Figure 4, with a constant and uniform timescale for loss
347 of 30 days (i.e., the lost rate was given as [CO]/30 molec cm^{-3} day^{-1}, where [CO] is the CO
348 concentration). We ran separate tracers for each of the continental regions, with each tracer
349 emitted only in that region but chemically destroyed everywhere.

350 The tracers were initialized to a uniformly low abundance of 1 pptv and the model was
351 run for 17 months prior to June 2004 to spinup the tracer distributions. Shown in Figure 5 are the
352 boundary layer (defined here as the surface – 700 hPa) and free tropospheric (700 – 250 hPa)
353 partial columns of the continental tracers for June 2004. In the extratropical northern hemisphere,
354 a larger fraction of the Asian surface emissions are exported to the free troposphere, compared to
355 the North American and European emissions. We find that transport of the Asian emissions to
356 the free troposphere is faster even in winter. In the tropics, transport of surface emissions to the
357 free troposphere is slowest for South America (not shown), most likley due to the fact that in
358 boreal summer the ITCZ is located in northern South America (in the northern hemisphere) and
359 hence transport of south American emissions to the southern subtropics and extratropics is
360 facilated instead by the influence of mid-latitude cyclones (Staudt et al., 2002). In fall, the ITCZ
361 moves south and convection over South America intensifies (Liu et al., 2010); as a result, we
362 find that, in December, the fraction of South American emissions in the free troposphere is
363 greater, and is comparable to that from northern Africa (not shown).

364 The monthly mean fraction of the global mass of each continental tracer that is in the
365 boundary layer and the free troposphere is listed in Table 2. North America and Europe have the

smallest mass fraction in the free troposphere, 26% and 21%, respectively. This suggests that, relative to the other continental regions, the air in the free troposphere from Europe and North America is older and more chemically aged. This is consistent with the results of Stohl et al. (2002), who examined the transport of idealized tracers from continental source regions using a Lagrangian particle dispersion model. They found that the European tracer was more confined to the lower troposphere, relative to the North American and Asian tracers. They also noted that "in terms of vertical transport, the North America tracer… behaves intermediately between the Asia and Europe tracers." This suggests that the surface layer and profile inversions are sampling sufficiently different air masses that they obtain different constraints on the North American and European source estimates. The surface layer inversion is sampling air that is less aged and should, therefore, be less susceptible to discrepancies in the OH abundance.

4.3. Influence of the OH distribution

In this section we compare the impact on the source estimates of the OH distribution from v8-02-01 of GEOS-Chem with that from our standard inversion (which is based on v5-07-08 of GEOS-Chem). As shown in Figure 6, v8-02-01 OH is significantly higher than on v5-07-08 in the Northern hemisphere, while it is much lower over South America and Indonesia.

Using the v8-02-01 OH fields, we repeated the profile and surface inversions for June – August 2004. Shown in Figure 7 are the scaling factors and their differences, based on the two versions of the OH fields. With v8-02-01 OH, the a posteriori emissions in the tropics changed only slightly, while the inferred emission estimates in the extratropics, mainly for North America and Europe, were much greater that those obtained with v5-07-08 OH. The regional source estimates are given in Table 3. For the contiguous United States, with v5-07-08 OH we inferred a June-August source of 25.4 Tg CO using the profile retrievals, whereas with v8-02-01 OH we

389 estimated a source of 49.2 Tg CO. Similarly, for Europe the source estimates inferred from the
390 profile inversion with v5-07-08 OH was 47.3 Tg, whereas with v8-02-01 OH it with was 68.3 Tg.

391 To help understand the differences in the regional source estimates shown in Table 3, the
392 mean CO lifetime in the tropics and in the northern midlatitudes, for August 2004, are plotted in
393 Figure 8. Throughout the lower and middle troposphere in the northern midlatitudes, the CO
394 lifetime is about 30% shorter with v8-02-01 OH, decreasing to less than 30 days between 900 –
395 400 hPa.. The shorter lifetime resulted in a reduction of the CO burden in the midlatitude free
396 troposphere. Consequently, greater extratropical a posteriori source estimates, relative to the v5-
397 07-08 OH inversions (see Table 3), were required to bring the model into agreement with the
398 MOPITT data. In Jiang et al. (2014), this change in the free tropospheric distribution of CO is
399 discussed further in the context of a regional inversion analysis for North American source
400 estimates. In the tropics, the CO lifetime increased by about 15% with v8-02-01 OH. However,
401 as shown in Figure 6, this reflects reductions in OH over source regions such as South America
402 and Indonesia, which are partially offset by increases in OH over northern tropical Africa and the
403 remote tropics. In general, we find that the relative differences between the source estimates
404 from the v8-02-01 and v5-07-08 OH inversions are smaller for the surface inversion compared to
405 the profile inversion, reflecting the fact the surface layer inversion is more strongly influenced by
406 fresh emissions and less by background CO in the free troposphere.

407 ## 5. Summary

408 We presented a global inversion analysis to quantify monthly mean CO source estimates
409 during the period of June 2004 – May 2005 using the version 5 MOPITT retrievals. Building on
410 the work of Jiang et al. (2013), we conducted a comparative analysis of the influence of the
411 MOPITT profile and surface layer retrievals on the inferred CO source estimates. The inversions

412 suggest a reduction in CO emission in the tropics, possible due to an overestimate of the biogenic
413 source of CO, and an increase in emissions at middle and high latitudes. In the northern
414 extratropics, we found that the inferred source estimates are typically much greater in winter than
415 in summer, consistent with the seasonality in CO emissions inferred by Kopacz et al. (2010).
416 With our standard OH distribution, we inferred source estimates of 148 Tg, 180 Tg, and 284 Tg
417 for the contiguous United States, Europe, and East Asia, respectively, using the surface layer
418 retrievals. Using the profile retrievals, the inferred source estimates were lower, 131 Tg, 158, and
419 282 Tg, respectively.

420 In general, we find that the annual mean, regional source estimates inferred from the
421 surface layer retrievals and those from the profile retrievals are in agreement to better than 10%,
422 with the exception of the North American (United States and Canada), European, and
423 Indian/southeast Asian estimates. The difference in the Indian/southeast Asian estimates is due to
424 discrepancies in vertical transport associated with the strong convective transport over the
425 Southeast Asian region (Jiang et al., 2013). For Europe and North America, we argue that the
426 differences in the source estimates from the profile and surface inversion are due to model
427 discrepancies in the free tropospheric abundance of CO from these regions. We conducted an
428 ideal tracer experiment and showed that transport of surface emissions from Europe and North
429 America to the free troposphere is slower than from other continental regions. Consequently,
430 compared to the inversion using the surface layer retrievals, the profile inversion is sampling
431 older, more chemically age air from North America and Europe in our simulation, and is,
432 therefore, more susceptible to discrepancies in long-range transport and in the chemical sink of
433 CO. This suggests that diagnostics to assess the age of air from the continental source regions
434 should be useful for interpreting the results from CO source inversions.

435 We examined the impact of the OH distribution on the inferred CO source estimates,
436 using OH fields from versions v5-07-08 and v8-02-01 of GEOS-Chem. We found that changing
437 OH from v5-07-08 (used in our standard inversions) to v8-02-01 produced large differences in
438 the extratropical source estimates. The relative differences in the source estimates from the
439 profile inversion using v5-07-08 and v8-02-01 OH were 64%, 33%, and 36% for source
440 estimates from the contiguous United States, East Asia, and Europe for June – August 2004,
441 when the CO lifetime is short. In the inversions using the surface layer data we found that the
442 impact of the OH fields was reduced, but was still large: 40%, 20%, and 24%, respectively. The
443 smaller impact of the OH fields in the surface layer inversion is due to the fact that the OH sink
444 is at a maximum in the middle troposphere, while the surface layer retrievals have maximum
445 sensitivity near the boundary layer.

446 The results presented here clearly demonstrate the challenge of inverse modeling of CO
447 emissions. Although the CO chemistry is relatively simple, the sensitivity to tropospheric OH is
448 a major issue. Accurate OH fields are essential for constraining CO reliably. In recent studies,
449 Fortems-Cheiney et al. (2011) introduced Methyl Chloroform (MCF) in their CO inversion to
450 provide a constaint on the OH abundnace. However, MCF is observed at only a few surface sites,
451 hence, although a MCF inversion might give a good global mean OH constraint, it will not help
452 mitigate discrepancies in the regional distribution of OH. A better method to improve the OH
453 would be to assimilate tropospheric ozone and it precursors, together with CO, as was done by
454 Miyazaki et al. (2012). They showed that in such a multispecies assimilation, the adjustment in
455 the monthly mean, zonal OH abundance could be as large as 20%.

456 Our inversion results also highlight the need to better quantify the isoprene source of CO.
457 Previous studies (e.g., Abbot et al., 2003; Shim et al., 2005; Millet et al., 2008) have used space-

458 based observatios of HCHO to inferred isoprene emissions. Since isoprene impacts the
459 tropopsheric abundance of OH and ozone, it may be that the most reliable constraint on the
460 isoprene source will be obtained by jointly assimilating HCHO data together with observations
461 of CO and other ozone precursors. In that context, Fortems-Cheiney et al. (2012) conducted a
462 joint inversion analysis using CO, HCHO, methane (CH_4), and MCF, and found that the biogenic
463 a priori source of CO was overestimated, whereas the a priori combustion source was
464 underestimated. Our results and those of Fortems-Cheiney et al. (2012) suggest that the way
465 forward will require exploiting a broader range of composition measurements, besides just that
466 of atmospheric CO, to better quantify the regional CO budget.

467 ## Appendix A: Indirect Validation of the MOPITT V5J Data

468 Although Deeter et al. (2012, 2013) showed that the bias in the V5 MOPITT data relative
469 to aircraft observation is small in the lower troposphere, we note that the aircraft data are limited
470 in space and time. Therefore, we conducted an indirect validation of the MOPITT data by
471 assimilating the data to optimize the modeled CO distribution and compared it with independent
472 data. A better understanding of potential bias in the data is critical for properly quantifying the
473 source estimates. Comparison of the CO distribution obtained with the a posteriori source
474 estimates can reveal potential bias in the inversion, but in that approach it is difficult to
475 determine whether the bias is in the data or the model. By constraining the modeled CO to match
476 the observations, we can more easily identify potential biases in the data. For example, recent
477 inversion studies (Arellano et al., 2006; Jones et al., 2009; Hooghiemstra et al. 2012) have shown
478 that the a posteriori CO emissions, inferred from MOPITT data, resulted in an overestimate of
479 CO abundances relative to surface in situ measurements. Hooghiemstra et al. (2012) suggested
480 that the overestimate of surface CO was due to a bias in the V4 MOPITT data that they

employed. However, Arellano et al. (2006) and Jones et al. (2009) used the V3 MOPITT product in their inversion analyses. Jiang et al. (2013) suggested that the bias seen by Hooghiemstra et al. (2012) could be due to discrepancies in vertical transport. We also note that MOPITT validation comparisons (Deeter et al., 2010; 2013) over land rely on NOAA aircraft in situ CO profiles that are concentrated in North America with only two out of 15 locations at latitudes higher than 50°N.

To assess potential bias in the MOPITT data set, we assimilated the MOPITT V5J CO profile data into the GEOS-Chem model using the sequential sub-optimal Kalman filter and compared the resulting CO field with GMD in situ surface CO observations. Figure A1 shows the comparison of the assimilated CO with monthly mean CO concentrations at selected GMD sites. We first compared the free model simulation (the standard GEOS-Chem simulation without Kalman filter assimilation) with GMD data. The initial condition for the free model run is the model original initial condition on June 1 2004, without optimization. In the northern hemisphere, the CO concentration of the free run model is higher than that of GMD in summer and fall, and significantly lower than that of GMD in winter and spring. In the southern hemisphere, the free run model generally overestimates the observed CO, which is consistent with previous studies (Shindell et al. 2006; Kopacz et al. 2010). In our assimilation, we first assimilated the MOPITT profile data between 60°S to 60°N. The result shows that the assimilated MOPITT data (dark blue dotted line) are highly consistent with the GMD data between 0°N to 30°N. However, the analysis has a positive bias in the mid-latitudes of the southern hemisphere and in the high latitudes of the north hemisphere, such as at Cold Bay (CBA), Alaska, and Mace Head (MHD), Ireland. In the southern hemisphere, at Crozet Island (CGO), the a priori is biased high and the assimilation exacerbated the bias. Although

Hooghiemstra et al. (2012) used V4 MOPITT data, our results suggests that the V5J data may also be biased high in the southern hemisphere. To reduce the potential impact of this high latitude bias in both hemispheres, we omitted MOPITT data in the assimilation that are polarward of 40° over oceans and 52° over land. As shown in Figure A1, this improved the agreement between the assimilated CO and the GMD data, but it did not completely remove the positive high-latitude bias at MHD and CGO. The results in Figure A1 show the value in the optimized initial conditions prior to the source estimation. The initial condition biases are much smaller than using original initial conditions from the free running model, particularly in winter and spring.

Appendix B: Optimization of the Cost Function

For the results presented here, the state vector in Equation (2) is not the CO emissions, but is a set scaling factors σ such that $\hat{\mathbf{x}} = \sigma \mathbf{x}_a$. Consequently, the optimization is conducted by minimizing the gradient of the cost function with respect to the scaling factors, with errors in the emission inventories assumed on a relative basis rather than on an absolute basis. In this approach, the gradient of the cost function as described in Equation (2) is usually scaled as follows:

$$\frac{\partial J}{\partial (x / x_a)} = \frac{\partial J}{\partial x} \cdot x_a \quad . \tag{B1}$$

This method is referred to as the linear scaling factor optimization. It assumes that the uncertainty in the emissions is normally distributed about scaling factor one. Henze et al. (2009) indicated that the normal distribution about one is nonphysical because it allows for negative emissions. An alternative method is the logarithm (LOG) scaling factor optimization (Henze et al., 2009):

$$\frac{\partial J}{\partial \ln(x/x_a)} = \frac{\partial J}{\partial x} \cdot x_a \cdot \frac{x}{x_a} \quad \text{(B2)}$$

It represents a log-normal distribution of scaling factors about zero. One advantage of LOG scaling factor optimization is that it can prevent negative scaling factors (Henze et al. 2009). However, it does not reduce negative gradients effectively because the increase in the factor x/x_a will partially offset the decrease of $\partial J/\partial x$. For example, assuming a negative gradient due to the model being lower than measurements (for example, $\partial J/\partial x = -100$), the inversion will increase emission (for example, $x/x_a = 1.5$) to reduce the negative gradient (for example, to $\partial J/\partial x = -66.7$). Using linear scaling factor optimization, we will see 33% improvement (reduction) of the gradient. However, using LOG scaling factor optimization, there is no improvement of the gradient because $\partial J/\partial x \times x/x_a = -66.7 \times 1.5 = -100$.

Figure B1 shows the results of the linear scaling optimization and the LOG optimization in a simulation experiment for April 2006. In the experiment, we created pseudo-observations by archiving the model output with the CO emissions unchanged (the default CO emission inventory). In the inversion analysis of the pseudo-data, we then reduce the CO emission by 50% so that the objective of the experiment is to produce scaling factors that can return the source estimate to the default emissions (i.e., scaling factors of 1.0). According to Equation (B1-B3), grids with strong CO emissions, such as those in East Asia, India, equatorial Africa and South America, will have a large initial gradient. Because the cost function is minimized in regions where the gradients are the largest, these strong emission regions will be optimized preferentially. After 30 iterations, the a posteriori estimate with linear method (Figure B1a) converges to the true state in all major emission regions. The results with LOG method are clearly worse (Figure B1b).

548 To better reduce the negative gradient, and avoid negative scaling factors, we developed
549 the following modification to the LOG method:

$$\begin{aligned} \frac{\partial J}{\partial \ln(x/x_a)} &= \frac{\partial J}{\partial x}\cdot x_a \cdot \frac{x}{x_a} \qquad when: \ \frac{x}{x_a} \le 1 \\ \frac{\partial J}{\partial \frac{1}{2}[(x/x_a)^2 - 1]} &= \frac{\partial J}{\partial x}\cdot x_a / \frac{x}{x_a} \qquad when: \ \frac{x}{x_a} > 1 \end{aligned} \tag{B3}$$

550

551 This new method is referred to as "LOGX2". It can minimize the positive and negative gradients
552 with comparable efficiency. As shown in Figure B1c, the optimization effect of the LOGX2
553 method is slightly better than that of the linear method. However, it should be noted that
554 although the LOGX2 approach improves the optimization efficiency and minimizes the potential
555 systematic errors, it impacts the statistics of the solution. With the linear or LOG approaches the
556 errors are Gaussian or log-normal, respectively, but with the LOGX2 scheme they are neither.

557 ## Acknowledgments.

558 This work was supported by funding from the Natural Science and Engineering Research
559 Council of Canada, the Canadian Space Agency, and NASA grant NNX10AT42G. We thank
560 NOAA ESRL for providing their CO flask data. We also thank the two anonymous reviewers for
561 their thoughtful and detailed comments on the manuscript.

562

563 ## 6. References

564 Abbot, D. S., Palmer, P. I., Martin, R. V., Chance, K. V., Jacob, D. J., and Guenther, A.:
565 Seasonal and interannual variability of North American isoprene emissions as determined by
566 formaldehyde column measurements from space, Geophys. Res. Lett., 30, 1886,
567 doi:10.1029/2003GL017336, 17, 2003.

568 Arellano, A. F. Jr. and Hess, P. G.: Sensitivity of top-down estimates of CO sources to GCTM
569 transport, Geophys. Res. Lett., 31, L21807, doi:10.1029/2006GL027371, 2006b.
570 Arellano, A. F. Jr., Kasibhatla, P. S., Giglio, L., van der Werf, G. R., Randerson, J. T., and
571 Collatz, G. J.: Time dependent inversion estimates of global biomass-burning CO emissions
572 using Measurement of Pollution in the Troposphere (MOPITT) measurements, J. Geophys.
573 Res., 111, D09303, doi:10.1029/2005JD006613, 2006.
574 Barkley, M. P., Palmer, P. I., Kuhn, U., Kesselmeier, J., Chance, K., Kurosu, T. P., Martin, R. V.,
575 Helmig, D. and Guenther, A.: Net ecosystem fluxes of isoprene over tropical South America
576 inferred from Global Ozone Monitoring Experiment (GOME) observations of HCHO columns,
577 J. Geophys. Res., 113, D20304, doi:10.1029/2008JD009863, 2008.
578 Deeter, M. N., Emmons, L. K., Francis, G. L., Edwards, D. P., Gille, J. C., Warner, J. X.,
579 Khattatov, B., Ziskin, D., Lamarque, J.-F., Ho, S.-P., Yudin, V., Attie, J.-L., Packman, D.,
580 Chen, J., Mao, D., and Drummond, J. R.: Operational carbon monoxide retrieval algorithm and
581 selected results for the MOPITT instrument, J. Geophys. Res., 108, 4399,
582 doi:10.1029/2002JD003186, D14, 2003.
583 Deeter, M. N., Edwards, D. P., Gille, J. C., Emmons, L. K., Francis, G., Ho, S.-P., Mao, D.,
584 Masters, D., Worden, H., Drummond, J. R., and Novelli, P. C.: The MOPITT version 4 CO
585 product: Algorithm enhancements, validation, and long-term stability, J. Geophys. Res., 115,
586 D07306, doi:10.1029/ 2009JD013005, 2010.
587 Deeter, M. N., Worden, H. M., Gille, J. C., Edwards, D. P., Mao, D., and Drummond, J. R.:
588 MOPITT multispectral CO retrievals: Origins and effects of geophysical radiance errors, J.
589 Geophys. Res., 116, D15303, doi:10.1029/2011JD015703, 2011.
590 Deeter, M. N., Worden, H. M., Edwards, D. P., Gille, J. C., and Andrews, A. E.: Evaluation of

591 MOPITT retrievals of lower-tropospheric carbon monoxide over the United States, J. Geophys.
592 Res., 117, D13306, doi:10.1029/2012JD017553, 2012.
593 Deeter, M. N., Martínez-Alonso, S., Edwards, D. P., Emmons, L. K., Gille, J. C., Worden, H. M.,
594 Pittman, J. V., Daube, B. C., and Wofsy, S. C.: Validation of MOPITT Version 5 thermal-
595 infrared, near-infrared, and multispectral carbon monoxide profile retrievals for 2000–2011, J.
596 Geophys. Res. Atmos., 118, 6710–6725, doi:10.1002/jgrd.50272, 2013.
597 Evans, M. J., and Jacob, D. J.: Impact of new laboratory studies of N_2O_5 hydrolysis on global
598 model budgets of tropospheric nitrogen oxides, ozone, and OH, Geophys. Res. Lett., 32,
599 L09813, doi:10.1029/2005GL022469, 2005.
600 Fortems-Cheiney, A., Chevallier, F., Pison, I., Bousquet, P., Szopa, S., Deeter, M. N., and
601 Clerbaux, C.: Ten years of CO emissions as seen from Measurements of Pollution in the
602 Troposphere (MOPITT), J. Geophys. Res., 116, D05304, doi:10.1029/2010JD014416, 2011.
603 Fortems-Cheiney, A., Chevallier, F., Pison, I., Bousquet, P., Saunois, M., Szopa, S., Cressot, C.,
604 Kurosu, T. P., Chance, K., and Fried, A., The formaldehyde budget as seen by a global-scale
605 multi-constraint and multi-species inversion system, Atmos. Chem. Phys., 12, 6699-6721,
606 doi:10.5194/acp-12-6699-2012, 2012.
607 George, M., et al.: Carbon monoxide distributions from the IASI/METOP mission: evaluation
608 with other space-borne remote sensors, Atmos. Chem. Phys., 9, 8317-8330, doi:10.5194/acp-9-
609 8317-2009, 2009.
610 Gonzi, S., Feng, L., and Palmer, P. I.: Seasonal cycle of emissions of CO inferred from MOPITT
611 profiles of CO: Sensitivity to pyroconvection and profile retrieval assumptions, Geophys. Res.
612 Lett., 38, L08813, doi:10.1029/2011GL046789, 2011.
613 Guenther, A., Karl, T., Harley, P., Wiedinmyer, C., Palmer, P.I., and Geron, C.: Estimates of

614 global terrestrial isoprene emissions using MEGAN (Model of Emissions of Gases and
615 Aerosols from Nature), Atmos. Chem. Phys., 6, 3181-3210, doi:10.5194/acp-6-3181-2006,
616 2006.
617 Heald, C. L., Jacob, D. J., Jones, D. B. A., Palmer, P. I., Logan ,J. A., Streets, D. G., Sachse, G.
618 W., Gille, J. C., Hoffman, R. N., and Nehrkorn, T.: Comparative inverse analysis of satellite
619 (MOPITT) and aircraft (TRACE-P) observations to estimate Asian sources of carbon monoxide,
620 J. Geophys. Res. 109, D23306, doi:10.1029/2004JD005185, 2004.
621 Henze, D. K., Hakami, A., and Seinfeld, J. H.: Development of the adjoint of GEOS- Chem,
622 Atmos. Chem. Phys.,7, 2413-2433, doi:10.5194/acp-7-2413-2007, 2007.
623 Henze, D. K., Seinfeld, J. H., and Shindell, D. T.: Inverse modeling and mapping US air quality
624 influences of inorganic PM2.5 precursor emissions using the adjoint of GEOS-Chem, Atmos.
625 Chem. Phys., 9, 5877-5903, doi:10.5194/acp-9-5877-2009, 2009.
626 Hooghiemstra, Krol, M. C., Bergamaschi, P., de Laat, A. T. J., van der Werf, G. R., Novelli, P.
627 C., Deeter, M. N., Aben, I., and Röckmann, T.: Comparing optimized CO emission estimates
628 using MOPITT or NOAA surface network observations, J. Geophys. Res. 117, D06309,
629 doi:10.1029/2011JD017043, 2012.
630 Hudman, R. C., Murray, L. T., Jacob, D. J., Millet, D. B., Turquety, S., Wu, S., Blake, D. R.,
631 Goldstein, A. H., Holloway, J., and Sachse, G. W.: Biogenic versus anthropogenic sources of
632 CO in the United States, Geophys. Res. Lett., 35, L04801, doi:10.1029/2007GL032393, 2008.
633 Jiang, Z., D. Jones, B. A., Kopacz, M., Liu, J., Henze, D. K., and Heald, C., Quantifying the
634 impact of model errors on top-down estimates of carbon monoxide emissions using satellite
635 observations, J. Geophys. Res., 116, D15306, doi:10.1029/2010JD015282, 2011.
636 Jiang, Z., Jones, D. B. A., Worden, H. M., Deeter, M. N., Henze, D. K., Worden, J., Bowman, K.

637 W., Brenninkmeijer, C. A. M., and Schuck, T. J.: Impact of model errors in convective
638 transport on CO source estimates inferred from MOPITT CO retrievals, J. Geophys. Res.
639 Atmos., 118, 2073–2083, doi:10.1002/jgrd.50216, 2013.
640 Jiang, Z., Jones, D. B. A., Henze, D., Worden, H., Wang, Y. X.: Regional data assimilation of
641 multi-spectral MOPITT observations of CO over North America, submitted to Atmos. Chem.
642 Phys, 2014.
643 Jones, D. B. A., Bowman, K. W., Logan, J. A., Heald, C. L., Liu, J., Luo, M., Worden, J., and
644 Drummond, J.: The zonal structure of tropical O_3 and CO as observed by the Tropospheric
645 Emission Spectrometer in November 2004 – Part 1: Inverse modeling of CO emissions, Atmos.
646 Chem. Phys., 9, 3547 – 3562, 2009.
647 Kopacz, M., Jacob, D. J., Henze, D. K., Heald, C. L., Streets, D. G., and Zhang, Q.: Comparison
648 of adjoint and analytical Bayesian inversion methods for constraining Asian sources of carbon
649 monoxide using satellite (MOPITT) measurements of CO columns, J. Geophys. Res., 114,
650 D04305, doi:10.1029/2007JD009264, 2009.
651 Kopacz, M., Jacob, D. J., Fisher, J. A., Logan, J. A., Zhang, L., Megretskaia, I. A., Yantosca, R.
652 M., Singh, K., Henze, D. K., Burrows, J. P., Buchwitz, M., Khlystova, I., McMillan, W. W.,
653 Gille, J. C., Edwards, D. P., Eldering, A., Thouret, V. and Nedelec, P.: Global estimates of CO
654 sources with high resolution by adjoint inversion of multiple satellite datasets (MOPITT, AIRS,
655 SCIAMACHY, TES), Atmos. Chem. Phys.,10, 855-876, doi:10.5194/acp-10-855-2010, 2010.
656 Kuhns, H., Green, M. and Etyemezian, V.: Big Bend Regional Aerosol and Visibility
657 Observational (BRAVO) Study Emissions Inventory, Report prepared for BRAVO Steering
658 Committee, Desert Research Institute, Las Vegas, Nevada, 2003.
659 Liu, J.-H., Logan, J. A., Jones, D. B. A., Livesey, N. J., Megretskaia, I., Carouge, C. and Nedelec,

P.: Analysis of CO in the tropical troposphere using Aura satellite data and the GEOS-Chem model: insights into transport characteristics of the GEOS meteorological products, Atmos. Chem. Phys., 10, 12207-12232, doi:10.5194/acp-10-12207-2010, 2010.

Luo, M., Rinsland, C. P., Rodgers, C. D., Logan, J. A., Worden, H., Kulawik, S., Eldering, A., Goldman, A., Shephard, M. W., Gunson, M. and Lampel, M.: Comparison of carbon monoxide measurements by TES and MOPITT: The influence of a priori data and instrument characteristics on nadir atmospheric species retrievals, J. Geophys. Res., 112, D09303, doi:10.1029/2006JD007663, 2007.

Marais, E. A., Jacob, D. J., Guenther, A., Chance, K., Kurosu, T. P., Murphy, J. G., Reeves, C. E., and Pye, H. O. T., Improved model of isoprene emissions in Africa using Ozone Monitoring Instrument (OMI) satellite observations of formaldehyde: implications for oxidants and particulate matter, Atmos. Chem. Phys., 14, 7693–7703, doi:10.5194/acp-14-7693-2014, 2014.

Millet, D. B., Jacob, D. J., Boersma, K. F., Fu, T.-M., Kurosu, T. P., Chance, K., Heald, C. L., Guenther, A.: Spatial distribution of isoprene emissions from North America derived from formaldehyde column measurements by the OMI satellite sensor, J. Geophys. Res., 113, D02307, doi:10.1029/2007JD008950, 2008.

Miyazaki, K., Eskes, H. J., Sudo, K., Takigawa, M., van Weele, M., and Boersma, K. F.: Simultaneous assimilation of satellite NO_2, O_3, CO, and HNO_3 data for the analysis of tropospheric chemical composition and emissions, Atmos. Chem. Phys., 12, 9545-9579, doi:10.5194/acp-12-9545-2012, 2012.

Olivier, J. G. J. and Berdowski, J. J. M.: Global emissions sources and sinks, in: The Climate System, edited by: Berdowski, J., Guicherit, R., and Heij, B. J., 33–78, A. A. Balkema Publishers/Swets & Zeitlinger Publishers, Lisse, the Netherlands, 2001.

683 Ott, L. E., Bacmeister, J., Pawson, S., Pickering, K., Stenchikov, G., Suarez, M., Huntrieser, H.,
684 Loewenstein, M., Lopez, J., and Xueref-Remy, I., Analysis of Convective Transport and
685 Parameter Sensitivity in a Single Column Version of the Goddard Earth Observation System,
686 Version 5, General Circulation Model, J. Atmos. Sci., 66, 627 – 646, DOI:
687 10.1175/2008JAS2694.1, 2009.
688 Palmer, P. I., Jacob, D. J., Jones, D. B. A., Heald, C. L., Yantosca, R. M., Logan, J. A. Sachse, G.
689 W. and Streets, D. G.: Inverting for emissions of carbon monoxide from Asia using aircraft
690 observations over the western Pacific, J. Geophys. Res., 108, 8828, doi:10.1029/2003JD003397,
691 D21., 2003.
692 Palmer, P. I., Suntharalingam, P., Jones, D. B. A., Jacob, D. J., Streets, D. G., Fu, Q., Vay, S. A.,
693 and Sachse, G. W.: Using CO_2:CO correlations to improve inverse analyses of carbon fluxes, J.
694 Geophys. Res., 111, D12318, doi:10.1029/2005JD006697, 2006.
695 Parrington, M., Jones, D. B. A., Bowman, K. W., Horowitz, L. W., Thompson, A. M., Tarasick,
696 D. W., and Witte, J. C.: Estimating the summertime tropospheric ozone distribution over North
697 America through assimilation of observations from the Tropospheric Emission Spectrometer, J.
698 Geophys. Res., 113, D18307, doi:10.1029/2007JD009341, 2008.
699 Parrington, M., Palmer, P. I., Henze, D. K., Tarasick, D. W., Hyer, E. J., Owen, R. C., Helmig,
700 D., Clerbaux, C., Bowman, K. W., Deeter, M. N., Barratt, E. M., Coheur, P.-F., Hurtmans, D.,
701 Jiang, Z., George, M. and Worden, J. R.: The influence of boreal biomass burning emissions on
702 the distribution of tropospheric ozone over North America and the North Atlantic during
703 2010, Atmos. Chem. Phys., 12, 2077-2098, doi:10.5194/acp-12-2077-2012, 2012.
704 Pétron, G., Granier, C., Khattatov, B., Yudin, V., Lamarque, J.-F., Emmons, L., Gille, J., and
705 Edwards, D. P.: Monthly CO surface sources inventory based on the 2000– 2001 MOPITT

706 satellite data, Geophys. Res. Lett., 31, L21107, doi:10.1029/2004GL020560, 2004.
707 Shim, C., Wang, Y.-H., Choi, Y., Palmer, P. I., Abbot, D. S. and Chance, K: Constraining global
708 isoprene emissions with Global Ozone Monitoring Experiment (GOME) formaldehyde column
709 measurements, J. Geophys. Res., 110, D24301, doi:10.1029/2004JD005629, 2005.
710 Shindell, D. T., Faluvegi, G., Stevenson, D. S., Krol, M. C., Emmons, L. K., Lamarque, J.-F.,
711 Petron, G., Dentener, F. J., Ellingsen, K., Schultz, M. G., Wild, O, Amann, M., Atherton, C. S.,
712 Bergmann, D. J., Bey, I., Butler, T., Cofala, J., Collins, W. J., Derwent, R. G., Doherty, R. M.,
713 Drevet, J., Eskes, H. J., Fiore, A. M., Gauss, M., Hauglustaine, D. A., Horowitz, L. W., Isaksen,
714 S. A., Lawrence, M. G., Montanaro, V., Muller, J.-F., Pitari, G., Parther, M. J., Pyle, J. A., Rast,
715 S., Rodriguez, J. M., Sanderson, M. G., Savage, N. H., Strahan, S. E., Sudo, K., Szopa, S.,
716 Unger, N., van Noije, T. P. C. and Zeng, G.: Multimodel simulations of carbon monoxide:
717 Comparison with observations and projected near-future changes, J. Geophys. Res., 111,
718 D19306, doi:10.1029/2006JD007100, 2006.
719 Singh, K., Jardak, M., Sandu, A., Bowman, K., Lee, M., and Jones, D.: Construction of non-
720 diagonal background error covariance matrices for global chemical data assimilation, Geosci.
721 Model Dev., 4, 299-316, doi:10.5194/gmd-4-299-2011, 2011.
722 Spivakovsky, C. M., Logan, J. A., Montzka, S. A., Balkanski, Y. J., Foreman-Fowler, M., Jones,
723 D. B. A., Horowitz, L. W., Fusco, A. C., Brenninkmeijer, C. A. M., Prather, M. J., Wofsy, S. C.
724 and McElroy, M. B.: Three-dimensional climatological distribution of tropospheric OH Update
725 and evaluation, J. Geophys. Res., 105(D7), 8931–8980, doi:10.1029/1999JD901006, 2000.
726 Staudt, A. C., Jacob, D. J., Logan, J. A., Bachiochi, D., Krishnamurti, T. N., and Poisson, N.:
727 Global chemical model analysis of biomass burning and lightning influences over the South
728 Pacific in austral spring, J. Geophys. Res., 107(D14), doi:10.1029/2000JD000296, 2002.
729 Stein, O., Schultz, M. G., Bouarar, I., Clark, H., Huijnen, V., Gaudel, A., George, M., and

730 Clerbaux, C.: On the wintertime low bias of Northern Hemisphere carbon monoxide found in
731 global model simulations, Atmos. Chem. Phys., 14, 9295-9316, doi:10.5194/acp-14-9295-2014,
732 2014.
733 Stohl, A., Eckhardt, S., Forster, C., James, P., and Spichtinger, N., On the pathways and
734 timescales of intercontinental air pollution transport, J. Geophys. Res., 107(D23), 4684,
735 doi:10.1029/2001JD001396, 2002.
736 Vestreng, V. and Klein, H.: Emission data reported to UNECE/EMEP. Quality assurance and
737 trend analysis and Presentation of WebDab, Norwegian Meteorological Institute, Oslo,
738 Norway, MSC-W Status Report, 2002.
739 van der Werf, G. R., Randerson, J. T., Giglio, L., Collatz, G. J., Mu, M., Kasibhatla, P. S.,
740 Morton, D. C., DeFries, R. S., Jin, Y., and van Leeuwen, T. T.: Global fire emissions and the
741 contribution of deforestation, savanna, forest, agricultural, and peat fires (1997–2009), Atmos.
742 Chem. Phys., 10, 11707–11735, doi:10.5194/acp-10-11707-2010, 2010.
743 Wang, H., Jacob, D. J., Kopacz, M., Jones, D. B. A., Suntharalingam, P., Fisher, J. A., Nassar, R.,
744 Pawson, S., and Nielsen, J. E.: Error correlation between CO_2 and CO as constraint for CO_2
745 flux inversions using satellite data, Atmos. Chem. Phys., 9, 7313-7323, doi:10.5194/acp-9-
746 7313-2009, 2009.
747 Warner, J., Comer, M. M., Barnet, C. D., McMillan, W. Wolf, W., Maddy, W., E., and Sachse,
748 G.: A comparison of satellite tropospheric carbon monoxide measurements from AIRS and
749 MOPITT during INTEX-NA, J. Geophys. Res., 112, D12S17, doi:10.1029/2006JD007925,
750 2007.
751 Worden, H. M., Deeter, M. N., Edwards, D. P., Gille, J. C., Drummond, J. R., and Nédélec, P.:
752 Observations of near-surface carbon monoxide from space using MOPITT multispectral

753 retrievals, J. Geophys. Res., 115, D18314, doi:10.1029/2010JD014242, 2010.
754 Worden, J., Jiang, Z., Jones, D. B. A., Alvarado, M., Bowman, K., Frankenberg, C., Kort, E. A.,
755 Kulawik, S. S., Lee, M.-M., Liu, J.-J., Payne, V., Wecht, K. and Worden, H.: El Nino, The
756 2006 Indonesian Peat Fires, And The Distribution Of Atmospheric Methane, Geophys. Res.
757 Lett., 40, 4938–4943, doi:10.1002/grl.50937, 2013.
758 Zhang, Q., Streets, D. G., Carmichael, G. R., He, K. B., Huo, H., Kannari, A., Klimont, Z., Park,
759 I. S., Reddy, S., Fu, J. S., Chen, D., Duan, L., Lei, Y., Wang, L. T., and Yao, Z. L.: Asian
760 emissions in 2006 for the NASA INTEX-B mission, Atmos. Chem. Phys., 9, 5131–5153,
761 doi:10.5194/acp-9-5131-2009, 2009.

762

763 **Tables and Figures**

764 **Table 1**. Annual total CO emission in different regions, from June 2004 to May 2005,
765 constrained by MOPITT surface level and tropospheric profile retrievals. The relative difference
766 on total (combustion + oxidation from biogenic VOCs) CO emission estimates is calculated by 2
767 * (CO_surface – CO_profile) / (CO_surface + CO_profile). The region defition is shown in
768 Figure 1.
769
770 **Table 2**. Monthly mean mass of continental CO tracers (Tg) in the boundary layer (lower
771 column) and the free troposphere (upper column). The upper fraction is calculated by
772 Mass_upper / Mass_total. The region defition is shown in Figure 4.
773
774 **Table 3**. Total CO emission in different regions, in Jun-Aug 2004, constrained by MOPITT
775 surface level and tropospheric profile retrievals. The region definition is shown in Figure 1.
776
777 **Figure 1**. Annual mean CO emissions from combustion sources and the oxidation of biogenic
778 NMVOC and CH_4, averaged from June 2004 to May 2005. The unit is 10^{12} molec/cm^2/sec. The
779 continental domains are defined with black boxes. The sub-continental domains in North
780 America (US, Mexico, Alaska and Canada) are seperated based on the country boundaries.
781
782 **Figure 2.** (a) – (e) Annual/Seasonal mean scaling factors, using MOPITT V5J surface level data;
783 (f) – (j) Annual/Seasonal mean scaling factors, using MOPITT V5J tropospheric profile data; (k)
784 – (o) Difference between two scaling factors, calculated by middle panel (e, f, g, h) minus left
785 panel (a, b, c, d).
786
787 **Figure 3.** Monthly variation of regional combustion CO emission estimates.

Figure 4. Distribution of emissions used for the idealized 30-day tracer. The unit is 10^{13} molec/cm^2/sec.

Figure 5. 30-day tracer partial columns in the extratropics for June 2004. The unit is 10^{18} molec/cm^2. Note the difference in scales between the lower and upper tropospheric columns.

Figure 6. (a, b): Mean tropospheric OH column (10^{12} molec/cm^2) in July 2004; (c,d): Meridional mean OH concentration (10^6 molec/cm^3) between 20°N-40°N in July 2004.

Figure 7. Scaling factors with MOPITT surface level retrievals and their difference. (a) – (c) Scaling factors, using v5-07-08 OH; (d) – (f) Scaling factors, using v8-02-01 OH; (i) – (l) Difference between two scaling factors.

Figure 8. Atmospheric CO lifetime averaged zonally at 30°N-50°N and 10°S-10°N for August 2004, estimated using v5-07-08 (black solid line) and v8-02-01 (red dash line) OH fields.

Figure A1. Annual variation of monthly mean CO concentration at selected GMD sites and surface level CO in GEOS-Chem, sampled at the GMD sites. Black solid line shows the GMD monthly mean CO. Red solid line shows the free model simulation with original initial condition. The blue dash line is the assimilation result using MOPITT from 60°S to 60°N. The green dash line is the assimilation result from excluding the high latitude data.

Figure B1. OSSE scaling factors for April 2006. The scaling factors represent the ratio of the estimated to true emissions. The ratio for the first guess is 0.5. The actual value is 1.0. Shown are the scaling factors obtained with: (a) the linear scaling factor optimization, (b) the LOG scaling factor optimization, (c) the LOGX2 scaling factor optimization.

	A Priori estimates (Tg/year)				Surface level inversion		Profile inversion		Relative differece between surface and profile inversion
Regions	Fossil fuel + Biofuel	Biomass burning	Total of Combustion	Oxidation from biogenic VOCs	Total of Combustion	Oxidation from biogenic VOCs	Total of Combustion	Oxidation from biogenic VOCs	
US 48 states	94	1	95	44	112	38	100	31	13%
Alaska and Canada	4	34	38	9	44	9	38	8	15%
Mexico	10	4	15	12	17	11	18	11	-5%
East Asia	171	9	180	51	233	51	233	50	0%
SE Asia/India	38	73	111	64	97	61	112	75	-17%
Australia	5	25	30	68	27	68	27	59	9%
Europe	98	3	101	28	142	37	126	31	13%
South America	44	71	114	184	102	135	99	125	6%
North Africa	47	79	126	121	104	95	101	90	4%
South Africa	19	97	116	79	101	69	104	71	-3%
Global	532	396	928	661	982	573	960	553	3%

Table 1. Annual total CO emission in different regions, from June 2004 to May 2005, constrained by MOPITT surface level and tropospheric profile retrievals. The relative difference on total (combustion + oxidation from biogenic VOCs) CO emission estimates is calculated by 2 * (CO_surface – CO_profile) / (CO_surface + CO_profile). The region defition is shown in Figure 1.

Tracer	Lower Col (Tg)	Upper Col (Tg)	Upper fraction (%)
North America	52	18	26
Europe	58	15	21
Asia	40	22	35
South America	40	22	35
North Africa	36	24	40
South Africa	34	20	37
Indonesia	31	24	43

Table 2. Monthly mean mass of continental CO tracers (Tg) in the boundary layer (lower column) and the free troposphere (upper column). The upper fraction is calculated by Mass_upper / Mass_total. The region defition is shown in Figure 4.

Regions	A Priori estimates (Tg/Jun-Aug)	v5-07-08 OH		v8-02-01 OH	
		Surface level inversion	Profile inversion	Surface level inversion	Profile inversion
US 48 states	50	37	25	55	49
Alaska and Canada	42	48	41	54	55
Mexico	7	4	3	5	4
East Asia	78	73	66	89	92
SE Asia/India	37	28	35	29	39
Australia	14	15	14	16	15
Europe	46	57	47	72	68
South America	75	67	52	68	54
North Africa	49	34	31	41	40
South Africa	77	61	60	65	63
Global	477	425	376	495	481

Table 3. Total CO emission in different regions, in Jun-Aug 2004, constrained by MOPITT surface level and tropospheric profile retrievals. The region definition is shown in Figure 1.

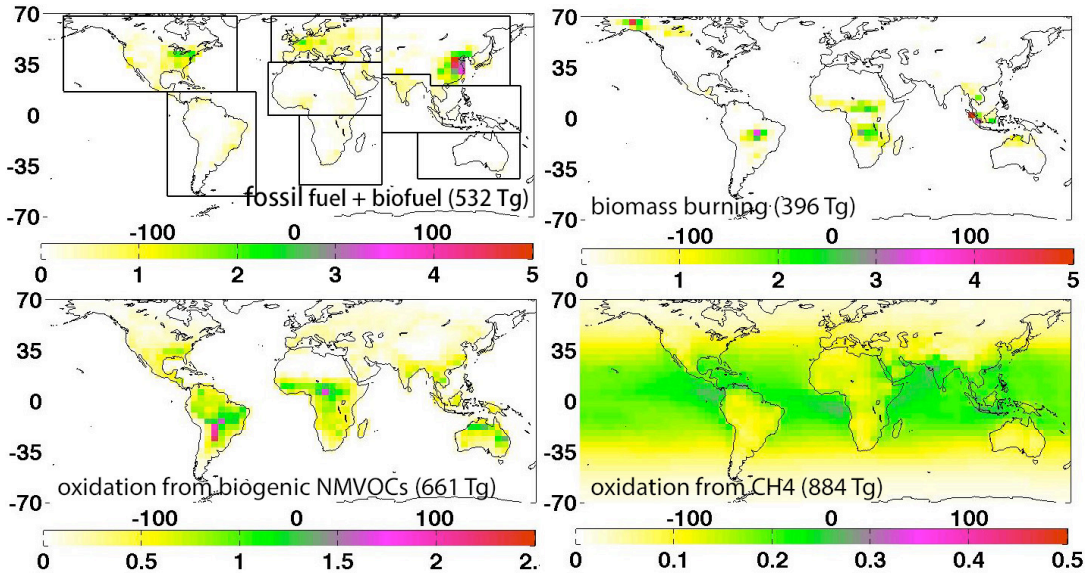

Figure 1. Annual mean CO emissions from combustion sources and the oxidation of biogenic NMVOC and CH_4, averaged from June 2004 to May 2005. The unit is 10^{12} molec/cm^2/sec. The continental domains are defined with black boxes. The sub-continental domains in North America (US, Mexico, Alaska and Canada) are seperated based on the country boundaries.

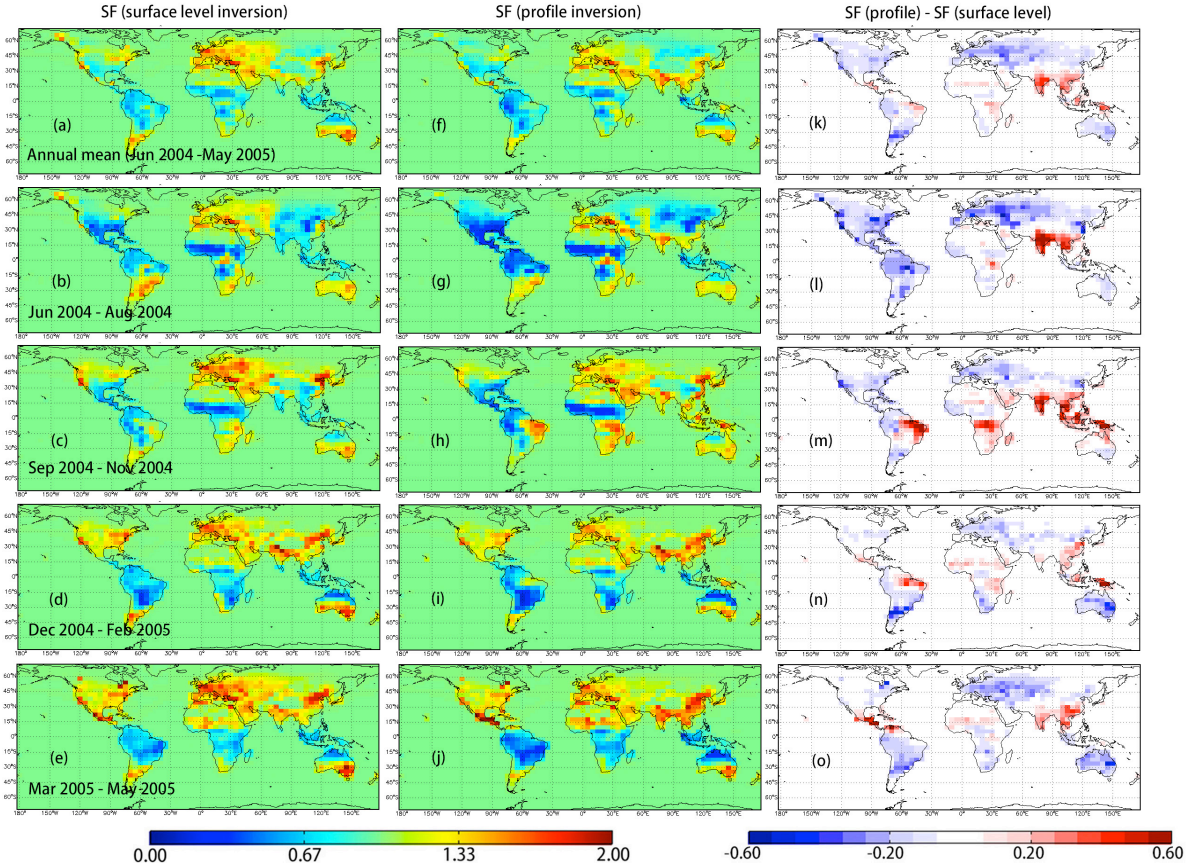

Figure 2. (a) – (e) Annual/Seasonal mean scaling factors, using MOPITT V5J surface level data; (f) – (j) Annual/Seasonal mean scaling factors, using MOPITT V5J tropospheric profile data; (k) – (o) Difference between two scaling factors, calculated by middle panel (e, f, g, h) minus left panel (a, b, c, d).

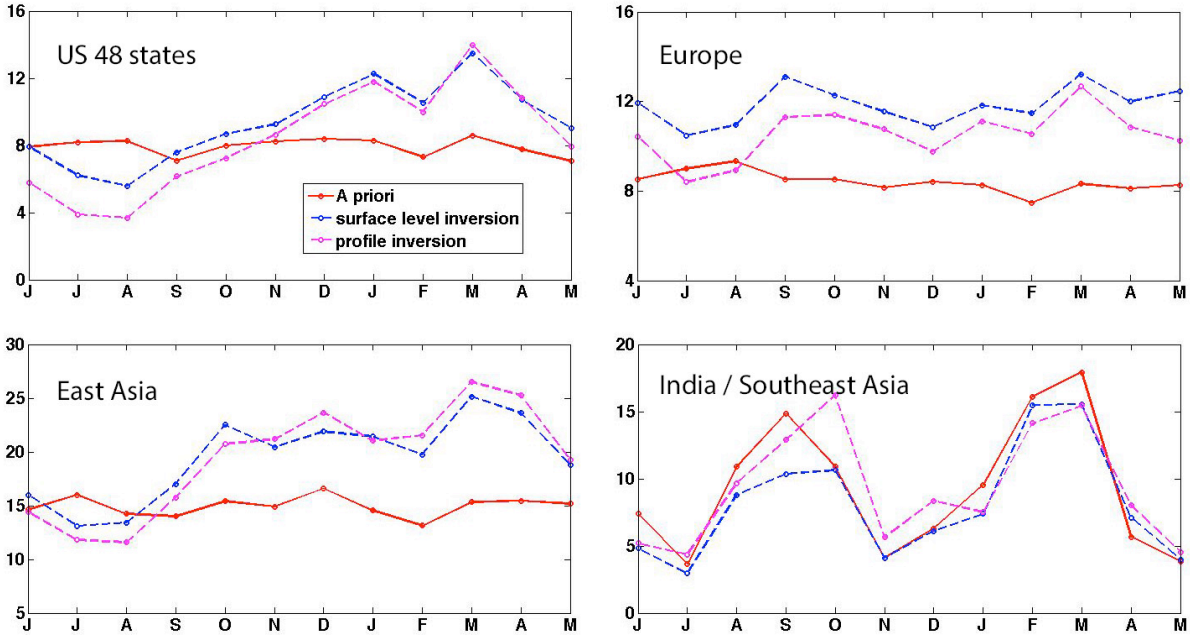

Figure 3. Monthly variation of regional combustion CO emission estimates.

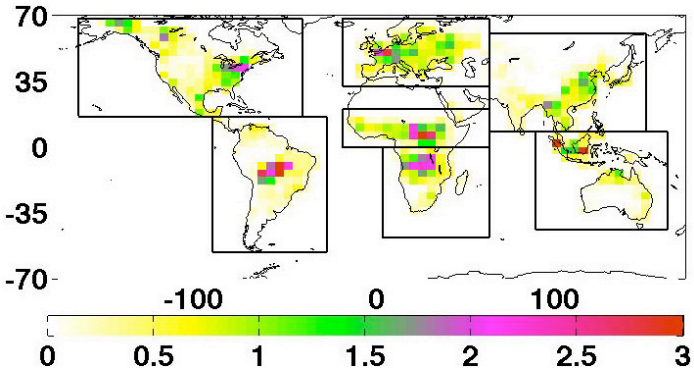

Figure 4. Distribution of emissions used for the idealized 30-day tracer. The unit is 10^{13} molec/cm^2/sec.

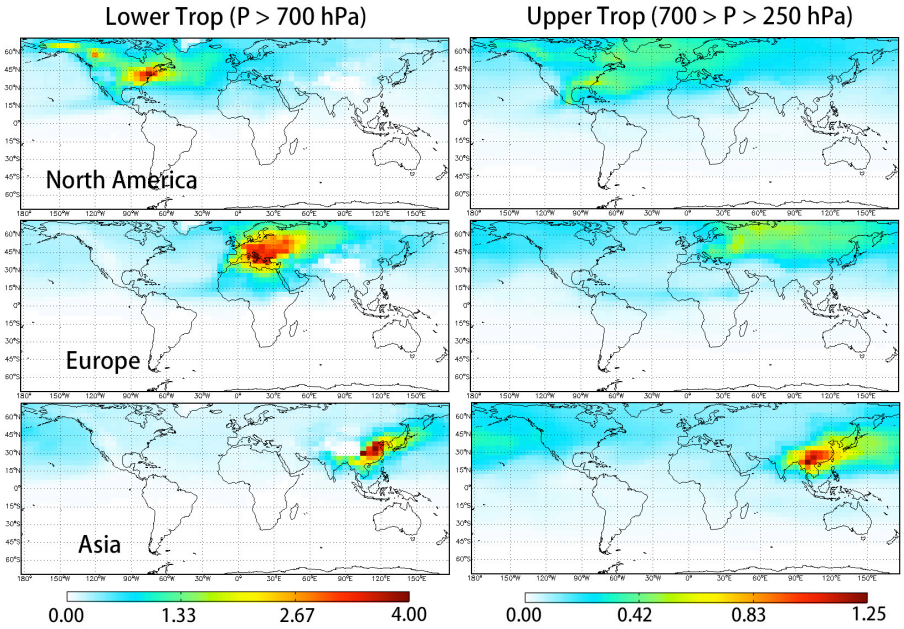

Figure 5. 30-day tracer partial columns in the extratropics for June 2004. The unit is 10^{18} molec/cm^2. Note the difference in scales between the lower and upper tropospheric columns.

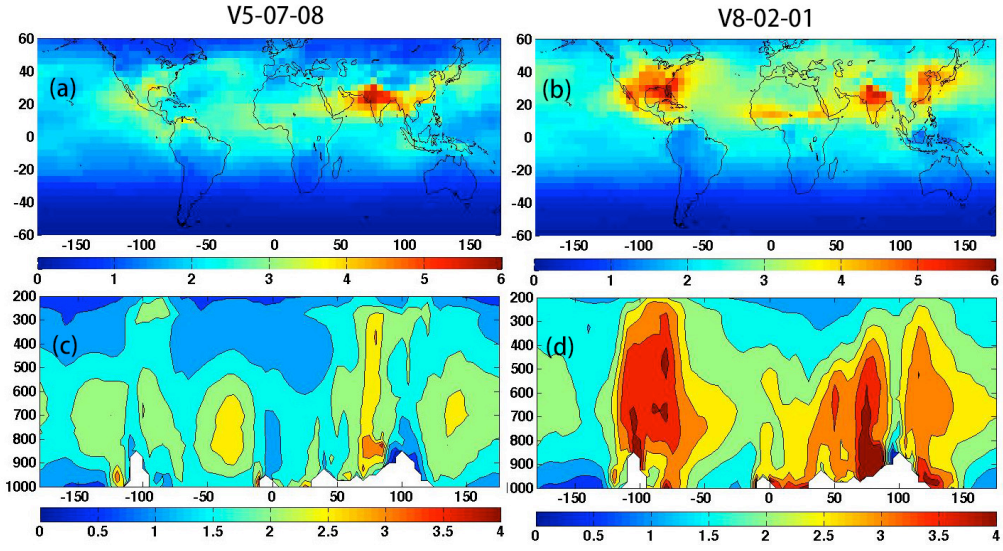

Figure 6. (a, b): Mean tropospheric OH column (10^{12} molec/cm^2) in July 2004; (c,d): Meridional mean OH concentration (10^6 molec/cm^3) between 20°N-40°N in July 2004.

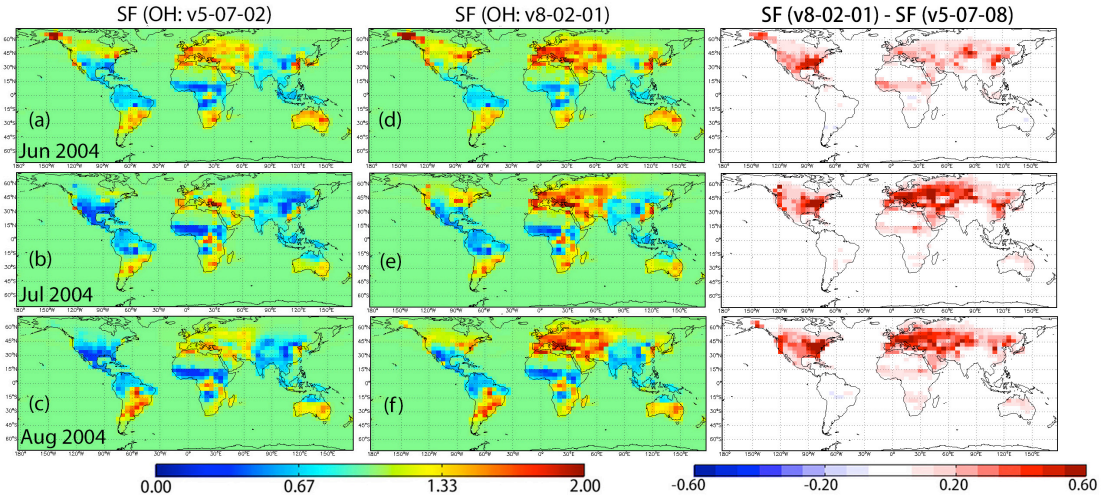

Figure 7. Scaling factors with MOPITT surface level retrievals and their difference. (a) – (c) Scaling factors, using v5-07-08 OH; (d) – (f) Scaling factors, using v8-02-01 OH; (i) – (l) Difference between two scaling factors.

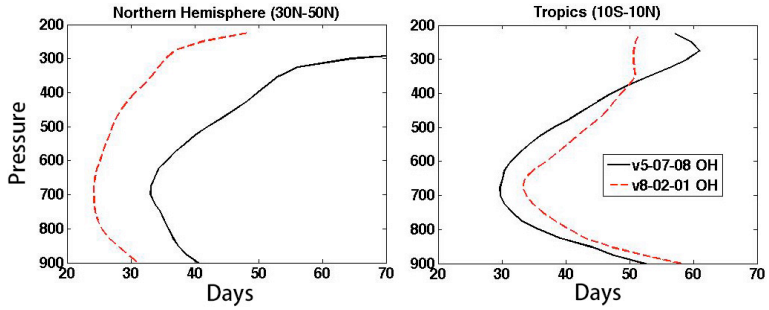

Figure 8. Atmospheric CO lifetime averaged zonally at 30°N-50°N and 10°S-10°N for August 2004, estimated using v5-07-08 (black solid line) and v8-02-01 (red dash line) OH fields.

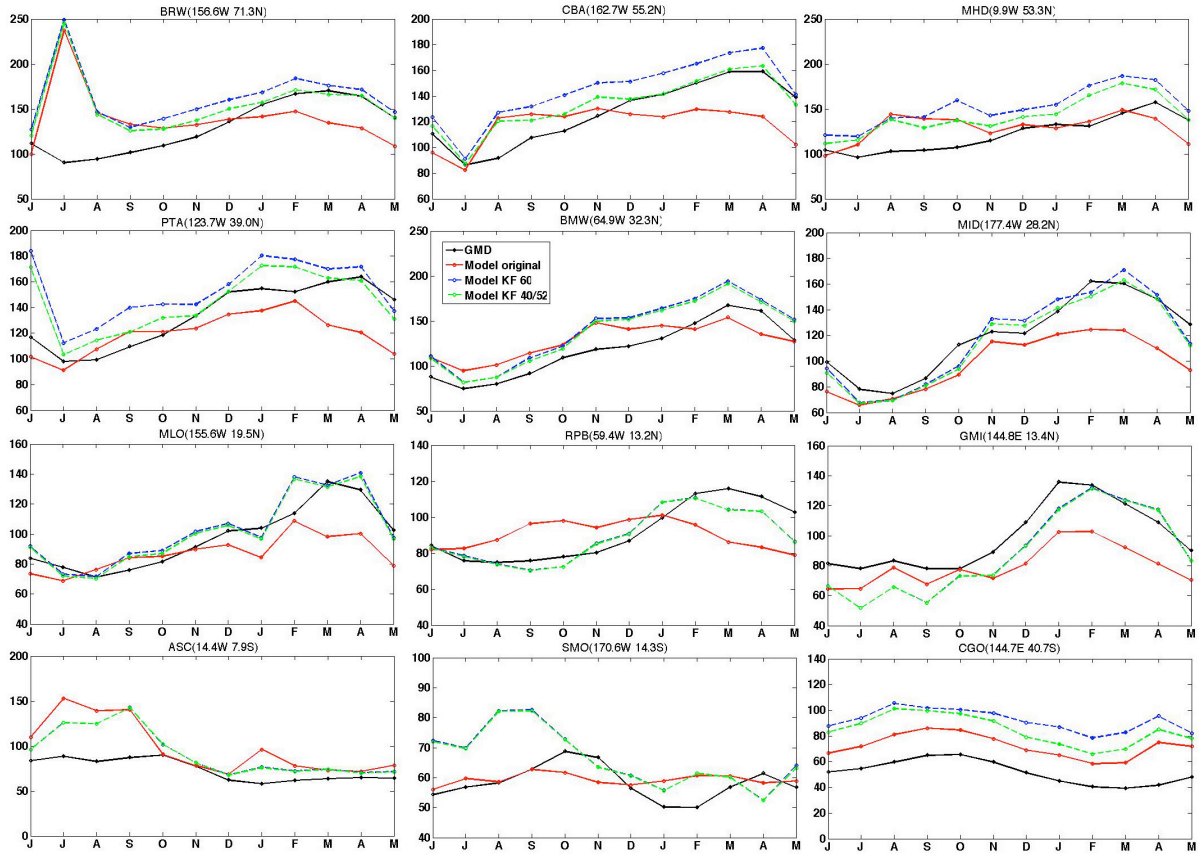

Figure A1. Annual variation of monthly mean CO concentration at selected GMD sites and surface level CO in GEOS-Chem, sampled at the GMD sites. Black solid line shows the GMD monthly mean CO. Red solid line shows the free model simulation with original initial condition. The blue dash line is the assimilation result using MOPITT from 60°S to 60°N. The green dash line is the assimilation result from excluding the high latitude data.

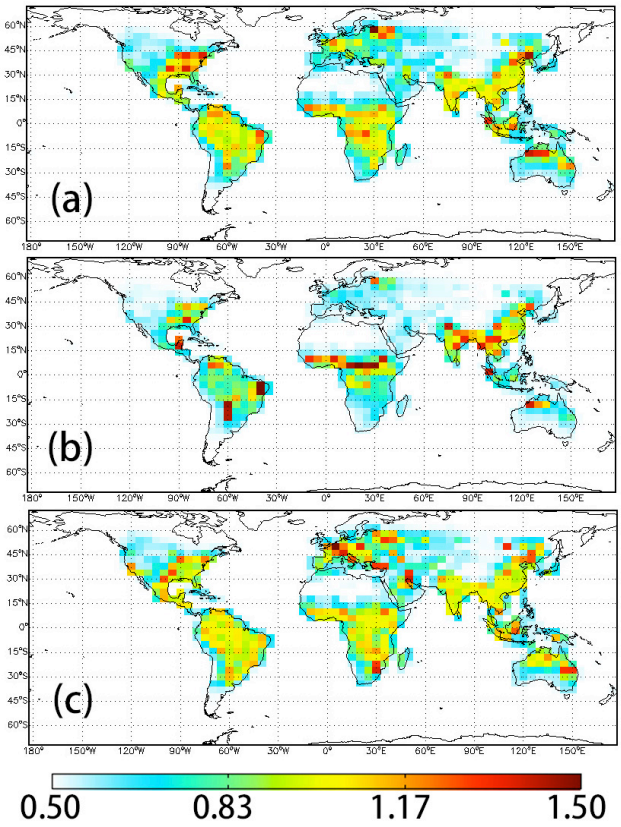

Figure B1. OSSE scaling factors for April 2006. The scaling factors represent the ratio of the estimated to true emissions. The ratio for the first guess is 0.5. The actual value is 1.0. Shown are the scaling factors obtained with: (a) the linear scaling factor optimization, (b) the LOG scaling factor optimization, (c) the LOGX2 scaling factor optimization.